

# Improving Lidar Based Tracking of UAVs Using an Approach Based on Focusing

Alberto Cerutti<sup>1</sup>, Sedat Dogru<sup>2</sup> and Lino Marques<sup>2</sup>

<sup>1</sup>Department of Electronics and Telecommunications (DET), Polytechnic University of Turin,  
10129 Turin, Italy s310131@studenti.polito.it

<sup>2</sup>Institute of Systems and Robotics, Department of Electrical and Computer Engineering,  
University of Coimbra, 3030-290 Coimbra, Portugal {sedat, lino}@isr.uc.pt

**Abstract**—This paper presents a novel approach for detecting drones using a lidar sensor integrated on a robotic turret. The turret rotates allowing the sensor to scan the sky, and both hardware components communicate in real-time. When the lidar sensor detects a drone, the detection data is used to dynamically adjust the motion pattern of the turret, allowing the system to capture more data by orienting the lidar sensor towards the drone, eventually improving tracking accuracy thanks to the higher number of detections achieved in this manner. In this paper we also explore different motion patterns for the turret, comparing them on the field to track a drone using the built lidar-turret system.

**Index Terms**—UAV, drone, detection, lidar, turret

## I. INTRODUCTION

In recent years, drones, also known as Unmanned Aerial Vehicles (UAVs), have seen widespread adoption, becoming increasingly common in civilian use across many countries for various applications. Small size, which allows easy carrying, user-friendly design, versatility of usage and improvements in related technologies, such as battery life, camera quality and stability during the flight, are key factors that contributed to this spreading. This can also be seen as a transformation from a military hardware to a civilian gadget and as a testament of how fast the technology is evolving. Since drones can easily be deployed for aerial images and videos, the private outdoor of one's house can be spied from the sky leading to direct violation of privacy [1]–[3]. The very low level of noise emitted by a drone both during take-off and during flight reduces the possibility of being noticed by unsuspecting citizens, facilitating even worse scenarios, such as that a crime can be committed without the victim ever noticing [4]. There have been cases of more dangerous drone usage in the past years, varying from destroying facilities, with repercussions on the worldwide economy [5], to killing people [6]–[8], or trying to kill [9]. To address these problems, the malicious drones should be at first detected and then somehow neutralized. In this work, we focus on the first part.

This work was financially supported by the AM2R project “Mobilizing Agenda for business innovation in the Two Wheels sector” funded by PRR - Recovery and Resilience Plan and by the Next Generation EU Funds, under reference C644866475-00000012 | 7253.

This work was performed during Erasmus stay of A. Cerutti at the University of Coimbra.

The research in this field led to different methods and sensors for drone detection, such as acoustic sensors, visible wavelength cameras, thermal infrared cameras, radar and lidar. Using acoustic sensors is a very cost-effective approach, because these sensors are most of the times cheaper than radars or thermal cameras. They also have weather resilience mainly to fog and change in light but also partially to rain, none interfering significantly with detections. However, the main obstacles to effective use of acoustic sensors are the presence of background noises, limited range and accuracy, and difficulty in detecting when multiple drones are flying at same time in the same environment [10]–[13]. Thermal infrared cameras allow the detection in conditions with low light intensity, for example during night flights outdoors or dark environments in closed environments. The thermal signatures are emitted primarily by batteries and in lower quantity, also by motors of the drones. Despite this advantage, infrared cameras have limited range of detection, and the possibility of interference with thermal sources from the background environment must be taken into account before choosing this solution [14], [15].

Continuous Wave Radar (CWR) is one of the most used methods to detect drones. It is affected neither by light intensity nor by weather conditions, so it is possible to detect drones with this method also during night and also under adverse weather conditions [16]. A CWR works by continuously transmitting an RF (Radio Frequency) signal which bounces back towards the radar when it encounters obstacles on its way. The CWR, upon receiving the reflected signals, analyzes the phase difference between the sent and received signals and hence determines the presence, the distance and the speed of the detected objects. CWRs allow a reliable measurement of the position even for moving objects. However, CWRs are sensitive to interference, which can lead to false positives. These false positives may be difficult to address in environments with a high density of obstacles, such as city centers, rendering them less suitable for applications in such environments [17], [18]. Lidars are sensors that can detect and very accurately localize drones during day and night. Previous works have proven the efficiency of lidar in tracking small drones due to the scanning performance and due to the range in which it can acquire data, ensuring that it is possible to protect an objective from drone threats in close range [19]. It was also shown that

lidars can be used to detect drones in ranges reaching 100 m [20]. However, performance of lidars deteriorates in foggy conditions. Another disadvantage of lidars is being able to instrument only a very small portion of the sky at a moment. Although this disadvantage is partially solved using 3D lidars with a high number of beams, they still leave parts of the sky unscanned, particularly at long ranges. It has been shown that a single frame may not provide enough data to detect a drone due to the resolution of the sensor [21]. A large amount of frames should be captured to accurately track the drone path, but it may not always be visible while flying in the sky. This paper uses a 3D lidar to detect and track drones, focusing on addressing the last disadvantage, particularly for tracking purposes. To accomplish this, a 3D lidar was installed on a robotic turret—also known as Pan-Tilt Unit (PTU)—with both the lidar and the PTU being controlled via a computer. In order to improve tracking performance, we propose several motion patterns for the turret and study their performance. We use a standard *sweeping* motion, in which the turret scans a predefined angular range at constant speed, as the baseline. Then we propose the following three motion patterns

- *Swinging*, the lidar rotates in a small range around the detected point
- *Stopping*, the lidar rests in the position in which the detection occurred
- *Slowing down*, the lidar after the detection rotates at a lower speed

All these types of motion are aimed at maintaining the drone visible to the lidar for longer, i.e. keeping it inside its field of view, and so they are aimed at capturing more frames of the drone moving in the environment, hopefully leading to better tracking performance.

## II. RELATED WORK

A reliable approach for detecting and tracking drones involves block-wise features and statistical analysis to capture acoustic signals emitted from drones [10]. From these audio signals it is possible to extract key features such as Short Time Energy, which contains the energy of small segments of the signal to analyze the variation of the intensity over time, Temporal Centroid to identify where the largest fraction of sound energy is concentrated, Zero Crossing Rate to count how many times the signal crosses the zero line and Mel-Frequency Cepstral Coefficients that contain the spectrum of the sound. These quantities are computed in short time periods (around 20 ms). After this first step, classification starts by using a one-class SVM (Support Vector Machine) where the largest amount of training data belongs to the drone acoustic emissions class and the objective is to keep them and get rid of the data belonging to the other class, which represent mostly the background noises. The one-class SVM learns the distribution of the drone acoustic emissions and constructs a boundary around this data in a higher-dimensional space. It then classifies new data points based on whether they fall inside or outside this boundary, aiming to identify and reject

outliers effectively. The goal is to minimize false positives and maximize true positive detections of the drone.

Another solution for drone detection is represented by CWR with the integration of Gaussian Mixture Model (GMM) [17]. The Radar continuously emits waves and collects data from the scanned environment, capturing both the positions of the fixed object and the moving ones, namely the drones. The GMM proceeds by modeling the background, which consists of processing the real-time data and constructing a probabilistic model of the background environment by using image pixels caught by the radar over time. The incoming radar pixels are classified based on their likelihood of belonging to the constructed background model. The ones that are considered to be inconsistent from the background are deemed to potentially be part of the drone. This step is done by setting a certain threshold to differentiate the drone from the background, generating a binary mask. During the post-processing part, the mask is refined to reduce noise and improve interference filtering.

Abir *et al.* [22] investigated the potential of applying a lidar sensor to detect and track drones under different conditions of the environment, paying particular attention to the intensity of the light and to the weather. Another factor that has been analyzed was the effect of drone size, shape and reflectivity on the lidar detections. In particular it came out that UAVs with higher reflectivity, such as the ones with lighter colors or with specific surface properties (such as details in metallic material), are easier to be detected than the ones characterized by dark and less reflective surfaces. Another factor that plays a significant role is the surface roughness: a smoother surface reflects more uniformly the incoming beams from the lidar, avoiding the unpredictable scattering seen with drones characterized by low surface finish. Uniform reflection is the key that makes drones with smoother surfaces easier to detect. Moreover, it is highlighted the good behavior of the lidar in real-time tracking, making it suitable for a wide range of fields [20], [23].

## III. BACKGROUND

### A. Lidar Sensor

A 3D lidar emits a large amount of pulses per second, it can measure the distance to multiple points and generate a point cloud that maps out the shape of the surrounding environment [24], [25]. Each point of the cloud has an own set of coordinates and it represents a portion of scanned object's surface. The point cloud is then processed for analysis, 3D reconstruction and modeling.

Some of the multibeam lidars use the same pulse sequence to fire the different sensors in the housing [25]. Fig. 1 shows the pulses, which also correspond to the firing sequence, of the VLP-16 lidar from Velodyne. Each of the 16 lasers are emitted and recharged once every  $55.296 \mu\text{s}$ . Specifically, every  $2.304 \mu\text{s}$  one of the laser sensors is fired, followed by an idle period of  $18.43 \mu\text{s}$ , resulting in a complete cycle time of  $55.296 \mu\text{s}$  for all lasers.

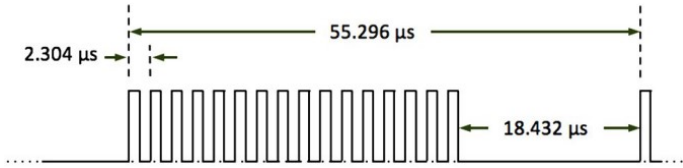


Fig. 1: Firing sequence timing of the Velodyne VLP-16 [25].

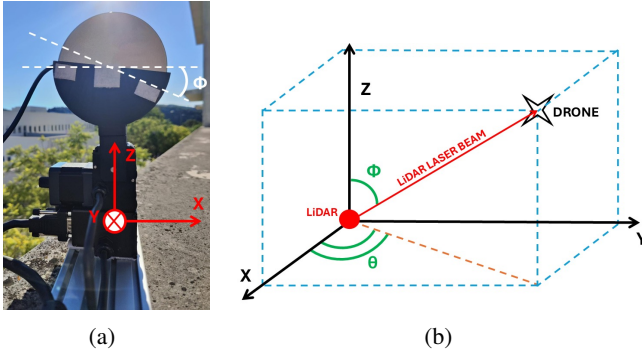


Fig. 2: (a) PTU with the lidar, and the corresponding world coordinates. (b) The PTU, the drone and the corresponding world coordinates.

### B. Detection

A 3D lidar scans the environment in its vertical and horizontal axes, providing much denser measurements in the second (Fig. 3). In our setup, the lidar is placed vertically on a pan-tilt unit (Fig. 2a). In this setup  $\theta$  represents the rotation of the turret around the z-axis (pan motion of the PTU), which we also refer to as yaw motion of the lidar, and  $\phi$  represents the internal rotation of the lidar, which we also refer to as the pitch angle (Fig. 2a).

The term *detection* refers to the ability of the lidar sensor to collect at least one data point from a flying drone. Due to the sparsity of the beams in both the vertical and horizontal axes and the pulsed nature mentioned above, detections are sparse and hence it is crucial to highlight the conditions that must be met for a detection to occur.

For detections to occur 3 conditions have to be met. One of the horizontal planes containing a beam of the lidar have to be aligned with the drone, the beam should align with the drone, and the beam should be fired. In other words the yaw angle of the beam and the azimuth angle of the drone with respect to the base should be almost equal, the pitch angle of the beam and the elevation angle of the drone with respect to the base should be almost equal, and the beam should be ON when the previous two conditions are met. The amount of *almost equal* depends on the size of the drone, and also size of the lidar beam.

In Fig. 4 we present an example for the conditions of detection. Fig. 4a illustrates the evolution of both the PTU pan angle and the drone azimuth angle over time during one of our field tests. The red path is taken from the ArduPilot logs from the drone itself, while the blue saw tooth plot represents the

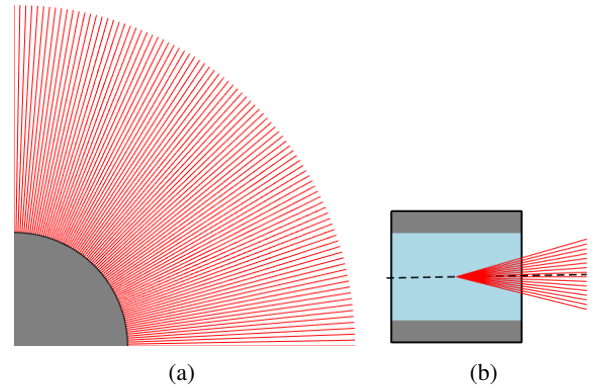


Fig. 3: (a) Partial view of the top of the lidar, with red showing the beams as the sensor inside the lidar rotates. (b) Side view of the lidar showing the 16 vertical beams in different planes.

yaw angle of the PTU, corresponding to one of the horizontal beams. At the time the PTU was sweeping left right at a constant speed. The plot can be divided into two sections: We are particularly interested in the intersections between the blue and red curves, as these represent the instances when the PTU, and thus the lidar mounted on top of it, is oriented towards the drone. Around 24 intersections can be seen in Fig. 4a. Closing in (Fig. 4b) we observe 4 intersections in a 22 s time window. Comparing the elevation angle of the drone and pitch angle of the beam with respect to the base (Fig. 4c, we observe intersections only at  $t = 231.683$  s. The red path, representing the drone elevation angle, appears flat in Fig. 4c because it displays a very short time period, about 0.02 s. Fig. 4e shows the last condition, where the pulse time and the intersections are matching, leading to a detection.

## IV. METHOD

To achieve our goal, the first stage is the detection of the target of interest. This step is followed by tracking process, meant as the continuous estimation of the target's position, whose estimate will be optimized by dynamically modifying the type of motion to which the lidar is subjected. The process aims at maximizing the number of times the drone remains inside the field of view of the lidar, ensuring it is visible for as long as possible. The current section will provide a detailed explanation of the working principles of each component, with a particular focus on the interactions between them. This includes the hardware components, ROS nodes, and the data exchanged between them. The implementation of the detection and identification mechanisms, alongside with the integration with the overall system, will be highlighted.

To facilitate the understanding of the components and their interactions, a block diagram is presented in Fig. 5. It illustrates the sequence and relationship between the various elements of the drone tracking system.

### A. Filter

The *Filter & Cluster* block takes as input the point cloud from the lidar and processes it through two consecutive

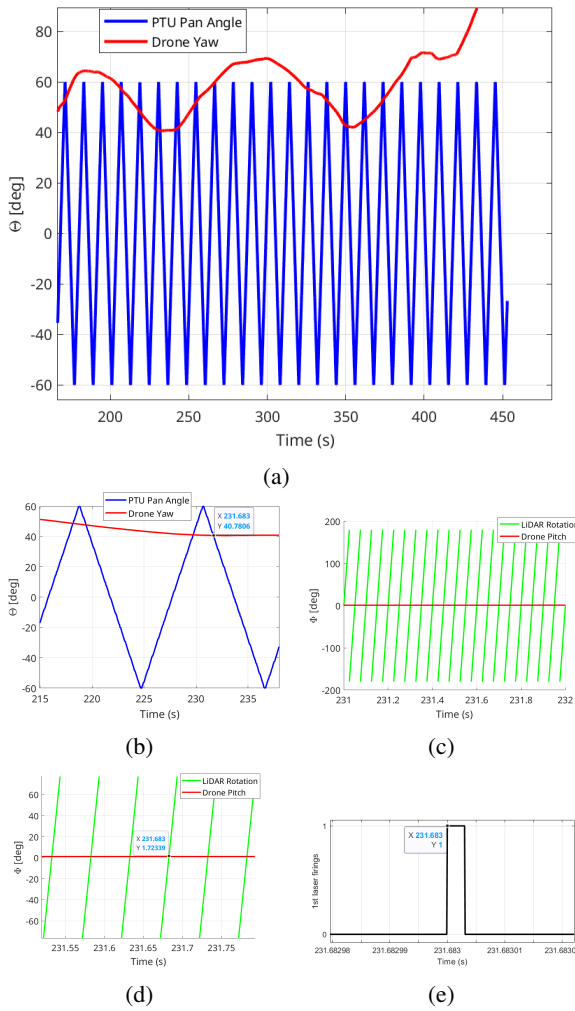


Fig. 4: (a) PTU pan angle and drone azimuth angle over time, (b) PTU pan angle and drone azimuth angle over time, zoom in, (c, d) lidar internal spin motion angle and drone elevation angle over time, zoom in at different scales, (e) lidar laser pulse firings, zoom in

filtering actions, namely an XYZ filter and a convex hull filter. The XYZ filter applies a quick thresholding to remove points that are not inside the Area of Interest (AoI). Then the left over points are passed through the convex hull filter, which accurately delineates the AoI. The AoI was selected large enough to contain the testing area of the drone, and these filters allow a quick way to remove the buildings, the trees, the street lamps and the ground in the outdoor testing area. Then left out clusters of point cloud are found and their centroids are calculated.

### B. Controller

The *controller* supports 4 different types of motion patterns:

- *Sweeping* This is the default motion pattern. The PTU continuously sweeps an angular range large enough to contain all the AoI.

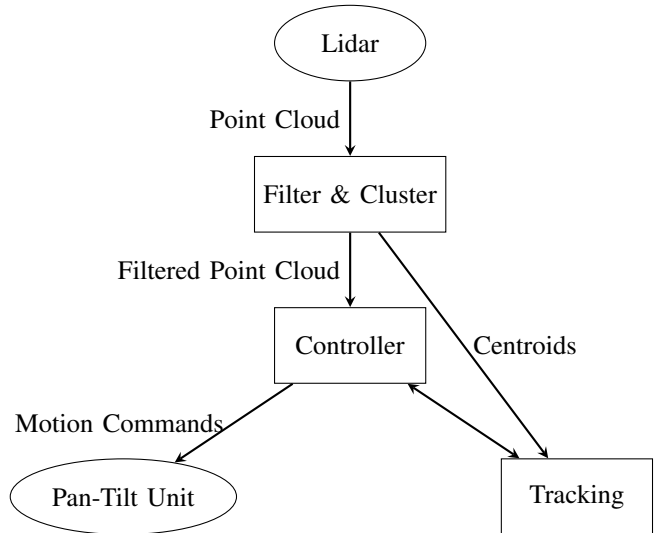


Fig. 5: Flowchart of the lidar data processing system

- *Swinging* The PTU oscillates between two closely spaced angles. These angles are found to be  $\pm\delta$ —around the azimuth angle of the drone with respect to the base of the PTU. The swinging happens a predefined  $n$  times, then *Sweeping* resumes.
- *Slow Down* The PTU’s speed is reduced by a scale factor, for  $\Delta\theta$  degrees. Then *Sweeping* resumes.
- *Stop*, stops the turret motion for  $\Delta t$  seconds before resuming its *Sweeping* rotation.

The last three motion patterns are triggered by a detection in the lidar, and at the end normal sweeping motion resumes.

### C. Tracking

The tracking node receives the centroid lidar data, and using this it constructs a track of the target drone. The first detection provides the position of the drone, and subsequent detections help improve accuracy of the position estimate and they also allow estimation of the speed. Taking into account the high accuracy of the lidar’s measurements, which result in accurate pose measurements, the tracking problem is assumed to be linear and hence a Kalman Filter is used for tracking. A constant speed model was used for the drone in this work. The filter is initialized with the centroid position, and then it alternates between *prediction* and *update* phases on each new measurement to refine the estimated state. The prediction phase uses a state transition model to predict the next state based on the previous state and the elapsed time. In the update phase, the filter incorporates the latest centroid measurement to correct the predicted state. In this work the state is defined to contain the position and velocity of the drone in 3D space, represented as a 6-dimensional vector,  $x_k$ . Tracking block also includes a mechanism to handle lost detections by checking the covariance matrix and elapsed time since the last detection. If the system detects that the object is lost, it re-initializes the

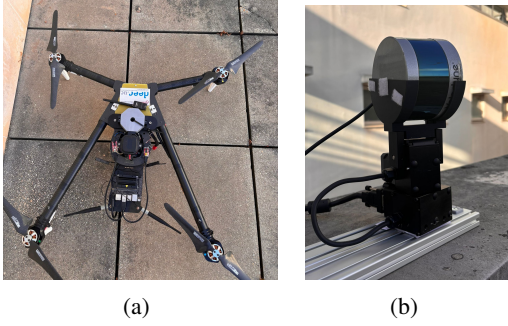


Fig. 6: (a) Sky Hero Spyder X4 drone (b) Tracking system

filter when a new centroid is detected. The filter equations are as follows:

$$\hat{x}_{k|k-1} = F\hat{x}_{k-1|k-1} \quad (1)$$

$$\hat{P}_{k|k-1} = F\hat{P}_{k-1|k-1}F^T + Q \quad (2)$$

$$e = z_k - H \cdot \hat{x}_{k|k-1} \quad (3)$$

$$S = H\hat{P}_{k|k-1}H^T + R \quad (4)$$

$$K = \hat{P}_{k|k-1} \cdot H^T S^{-1} \quad (5)$$

$$\hat{x}_{k|k} = \hat{x}_{k|k-1} + Ke \quad (6)$$

$$\hat{P}_{k|k} = (I - K \cdot H)\hat{P}_{k|k-1} \quad (7)$$

The predicted state estimate at time  $k$  given observations up to time  $k - 1$  is represented by  $\hat{x}_{k|k-1}$ , while  $\hat{P}_{k|k-1}$  denotes the predicted error covariance matrix. The state transition matrix  $F$  describes how the state evolves from the previous time step, and the process noise covariance matrix  $Q = \text{diag}(0.01, 0.01, 0.01, 0.01, 0.01, 0.01)$  captures uncertainty due to process noise. The innovation, or measurement residual  $e$ , quantifies the difference between the actual measurement  $z_k$  and the predicted measurement. The observation matrix  $H$  relates the state to the observed measurements, and the innovation covariance matrix  $S$  assesses uncertainty, influenced by the measurement noise covariance  $R = \text{diag}((1)^2, (1)^2, (0.2)^2)$ . The Kalman gain  $K$  determines how much the predicted state estimate is adjusted based on the measurement residual, while the identity matrix  $I$  is used in calculating the updated error covariance. After incorporating  $z_k$ , the updated state estimate at time  $k$  is given by  $\hat{x}_{k|k}$ , and the corresponding updated error covariance matrix is represented by  $\hat{P}_{k|k}$ .

## V. EXPERIMENTAL SETUP

In this work a Sky Hero Spyder X4 with a 0.85-meter carbon fiber frame was used as the target drone (Fig. 6a). The drone has a Drotek DP0601 GNSS receiver with an external GNSS antenna, a Drotek RM3100 compass and two inertial measurement units (IMUs).

For detection, a three component system consisting of a pan-tilt unit, a 3D lidar and a 3D printed support was used (Fig. 6b). The PTU supports up to 4 kg payload, achieves speeds higher than  $300^\circ$  per second, with a resolution of about  $0.129^\circ$ . The lidar is a VLP-16 from Velodyne, with

100 m range, and  $360^\circ$  horizontal and  $32^\circ$  vertical field of view. The described method was implemented using C++ and ROS framework, with each block being a different ROS node. The drone itself was flown along the same pre-programmed trajectory for each test. The experiment data was saved as bag files and csv files, allowing later replay of the mission plot of the results.

## VI. RESULTS AND DISCUSSIONS

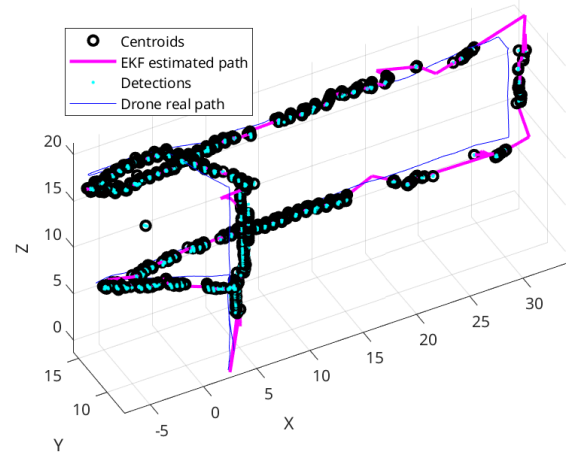


Fig. 7: Tracking of drone path, with *swinging* motion

Fig. 7 shows the path of the drone (taken from GNSS), the corresponding laser detections and the path estimated using KF for one of the test runs on the field during a test flight tracked with the *swinging* motion. The cyan points represent all the points that are selected during the filtering step, while the black circles figure the centroids. When detections are denser, the KF provides a more accurate path because a higher number of received centroids leads to increase in the frequency of the update steps: each of them refines the state estimate by including new measurements, reducing uncertainty and improving the precision of the drone's estimated path.

Fig. 8 and Fig. 9 show how the drone's position evolves along the XYZ coordinates with respect to time for different PTU motion patterns.

It is noticeable that the magenta path, indicating the estimated drone path by the KF, is smoother in the swinging case shown in Fig.8, with fewer jumps. This can be explained by the fact that a higher number of update steps allows for a more precise estimation of the drone's movement, resulting in better tracking.

Another analysis can be conducted on the density of detections over time, highlighting how many of the 16 beams are detecting the drone. The more beams detecting the drone, the more accurate the estimated data will be. This data is presented for the first half of the flights in Fig. 10. In these four flights the drone performed the same missions (shown in Fig. 7), and hence the detections are comparable for the different motion

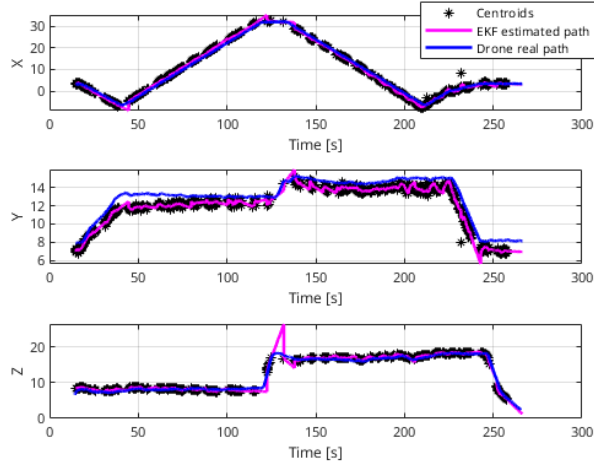


Fig. 8: Tracking over time, *swinging* approach

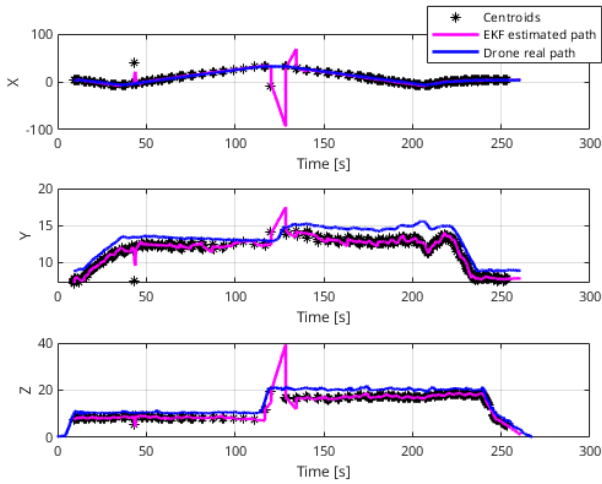


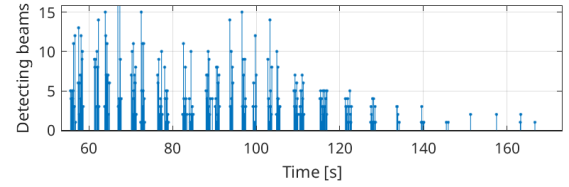
Fig. 9: Tracking over time, *sweeping* approach

patterns of the PTU. A common trend is visible in all motion patterns. Detections are more concentrated at the beginning, because the drone took off in front of the lidar at a short distance and moved away. Close take-off made it easy to detect frequently and with a high number of beams. As the drone moved further away from the sensor, it was harder to detect due to the spatial sparsity of the beams, resulting in a lower number of detections.

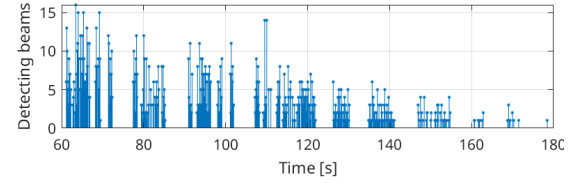
Comparing the graphs, it is evident that different motion patterns result in different detection density and patterns. *Sweeping* can be seen to detect more uniformly but also have fewer detections. *Stop* can be seen to detect for longer at a time, but it is less uniform. This observation is supported also by the number of detections presented on Table I. *Stopping* reports 4871 detections whereas *Sweeping* reports 2564 detections. On the other hand, the maximum time between detections is 10.6s for *Stopping* and 8.2s for *Sweeping*. *Swinging* and

TABLE I: Performance of Different Detection Strategies

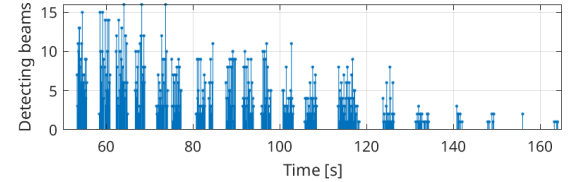
	Sweeping	Swinging	Slowing down	Stopping
Number of detections	2564	3182	3615	4871
Time between detections				
Minimum (s)	0.0717	0.0650	0.0637	0.0665
Maximum (s)	8.21	6.95	7.29	10.6
Mean (s)	0.409	0.303	0.286	0.208
3D Estimate Error (m)	3.23	1.44	1.56	1.50



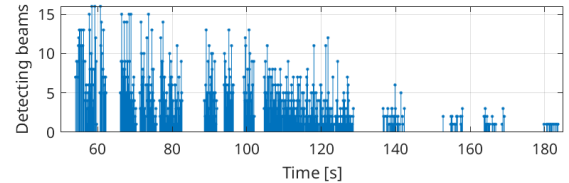
(a)



(b)



(c)



(d)

Fig. 10: Number of detections for different motion patterns of the PTU (a) sweeping (b) swinging (c) slow down (d) stop

*Slowing down* report more detections than *Sweeping* and less than *Stopping* and they both excel in reducing maximum time between detections, at 6.9s and 7.3s respectively.

Table I also shows the mean error in the estimated position of the drone, calculated comparing the GNSS position ( $x_{\text{GNSS}}$ ) of the drone with the KF position ( $x_{\text{KF}}$ ) using the formula

$$d = \frac{1}{N} \sum_{k=1}^N \|x_{\text{KF}} - x_{\text{GNSS}}\| \quad (8)$$

*Sweeping* can be seen to have the worst average estimate error, whereas the other three strategies have an error around 1.5 m, with *Swinging* achieving the best tracking performance of 1.44 m.

## VII. CONCLUSION

The research presented in this paper focused on the optimization of drone tracking using lidar sensor, specifically exploring the efficacy of different motion patterns: sweeping, swinging, slow-down, and stopping, from which swinging emerges as the most effective strategy in terms of estimation error. This motion pattern enhances detection by concentrating the lidar's scanning action on the specific area around the drone position, consequently improving tracking accuracy and reducing uncertainty in position estimation. We plan to test further the proposed motion strategies, validating them for more complex drone paths.

## REFERENCES

- [1] S. Rice. "Eyes in the sky: The public has privacy concerns about drones." *Forbes.com*. Accessed: Oct. 7, 2024. [Online]. Available: <https://www.forbes.com/sites/stephenrice1/2019/02/04/eyes-in-the-sky-the-public-has-privacy-concerns-about-drones/>
- [2] N. Thornton. "Privacy and drones: An invasion from the skies unveiled - protect your rights now!" *PrivacyEnd*. Accessed: Oct. 7, 2024. [Online]. Available: <https://www.privacyend.com/privacy-drones-invasion-skies/>
- [3] "Drones: The latest threat to the right to privacy." *The National Judicial College*. Accessed: Oct. 7, 2024. [Online]. Available: <https://www.judges.org/news-and-info/drones-latest-threat-right-privacy/>
- [4] V. Swales. "Drones used in crime fly under the law's radar." *The New York Times*. Accessed: Oct. 7, 2024. [Online]. Available: <https://www.nytimes.com/2019/11/03/us/drones-crime.html>
- [5] B. Hubbard, P. Karasz, and S. Reed. "Two major Saudi oil installations hit by drone strike, and U.S. blames Iran." *The New York Times*. Accessed: Oct. 7, 2024. [Online]. Available: <https://www.nytimes.com/2019/09/14/world/middleeast/saudi-arabia-refineries-drone-attack.html>
- [6] E. Peltier, E. Schmitt, and I. Alfa. "Errant airstrikes by Nigeria's military have killed worshipers, herders and refugees." *The New York Times*. Accessed: Oct. 7, 2024. [Online]. Available: <https://www.nytimes.com/2023/12/12/world/africa/nigeria-military-air-strikes.html>
- [7] T. Qiblawi. "A drone attack in Abu Dhabi could mark a dangerous turning point for the Middle East." *CNN.com*. Accessed: Oct. 7, 2024. [Online]. Available: <https://edition.cnn.com/2022/01/18/middleeast/uae-abu-dhabi-houthi-yemen-explainer-intl/index.html>
- [8] "Mali: Drone strikes killed 13 civilians including seven children in Amasrakad." *Amnesty International*. Accessed: Oct. 7, 2024. [Online]. Available: <https://www.amnesty.org/en/latest/news/2024/03/civilians-seeking-shelter-were-killed-by-drone-strike-in-town-in-gao-region/>
- [9] "A closer look at the drone attack on Maduro in Venezuela." *The New York Times*. Accessed: Oct. 7, 2024. [Online]. Available: <https://www.nytimes.com/2018/08/10/world/americas/venezuela-video-analysis.html>
- [10] M. Ohlenbusch, A. Ahrens, C. Rollwage, and J. Bitzer, "Robust drone detection for acoustic monitoring applications," in *2020 28th European Signal Processing Conference (EUSIPCO)*, 2021, pp. 6–10.
- [11] A. Sedunov, H. Salloum, A. Sutin, N. Sedunov, and S. Tsyuryupa, "UAV passive acoustic detection," in *2018 IEEE International Symposium on Technologies for Homeland Security (HST)*, 2018, pp. 1–6.
- [12] B. Harvey and S. O'Young, "Acoustic detection of a fixed-wing UAV," *Drones*, vol. 2, no. 1, 2018.
- [13] L. Liu, B. Sun, J. Li, R. Ma, G. Li, and L. Zhang, "Time-frequency analysis and recognition for UAVs based on acoustic signals collected by low-frequency acoustic-electric sensor," *IEEE Sensors Journal*, vol. 24, no. 12, pp. 19 601–19 613, June 2024.
- [14] P. Andrašić, T. Radišić, M. Muštra, and J. Ivošević, "Night-time detection of uavs using thermal infrared camera," *Transportation Research Procedia*, vol. 28, pp. 183–190, 2017, iNAIR 2017.
- [15] A. Thomas, V. Leboucher, A. Cotinat, P. Finet, and M. Gilbert, "UAV localization using panoramic thermal cameras," in *Computer Vision Systems*, D. Tzovaras, D. Giakoumis, M. Vincze, and A. Argyros, Eds. Cham: Springer International Publishing, 2019, pp. 754–767.
- [16] M. Pieraccini, L. Miccinesi, and N. Rohjani, "A doppler range compensation for step-frequency continuous-wave radar for detecting small UAV," *Sensors*, vol. 19, no. 6, 2019.
- [17] C. Liang, N. Cao, X. Lu, and Y. Ye, "UAV detection using continuous wave radar," in *2018 IEEE International Conference on Information Communication and Signal Processing (ICICSP)*, 2018, pp. 1–5.
- [18] A. Moses, M. J. Rutherford, and K. P. Valavanis, "Radar-based detection and identification for miniature air vehicles," in *2011 IEEE International Conference on Control Applications (CCA)*, 2011, pp. 933–940.
- [19] M. Hammer, M. Hebel, M. Laurenzis, and M. Arens, "Lidar-based detection and tracking of small UAVs," in *Emerging Imaging and Sensing Technologies for Security and Defence III; and Unmanned Sensors, Systems, and Countermeasures*, G. S. Buller, R. C. Hollins, R. A. Lamb, and M. Mueller, Eds., vol. 10799, International Society for Optics and Photonics. SPIE, 2018, p. 107990S.
- [20] S. Dogru and L. Marques, "Drone detection using sparse lidar measurements," *IEEE Robotics and Automation Letters*, vol. 7, no. 2, pp. 3062–3069, 2022.
- [21] M. Hammer, M. Hebel, B. Borgmann, M. Laurenzis, and M. Arens, "Potential of lidar sensors for the detection of UAVs," in *Laser Radar Technology and Applications XXIII*, M. D. Turner and G. W. Kamerman, Eds., vol. 10636, International Society for Optics and Photonics. SPIE, 2018, p. 1063605.
- [22] T. A. Abir, E. Kuantama, R. Han, J. Dawes, R. Mildren, and P. Nguyen, "Towards robust lidar-based 3d detection and tracking of UAVs," in *Proceedings of the Ninth Workshop on Micro Aerial Vehicle Networks, Systems, and Applications*, ser. DroNet '23. New York, NY, USA: Association for Computing Machinery, 2023, p. 1–7.
- [23] A. Quantel, "A scanning LiDAR for long range detection and tracking of UAVs," *Theses*, Normandie Université, Jan. 2021.
- [24] G. Vosselman and H. Maas, *Airborne and Terrestrial Laser Scanning*. Whittles Publishing, 2010.
- [25] *VLP-16 User Manual*, Velodyne LiDAR Inc.